IPEM
Institute of Physics and
Engineering in Medicine

Application of the phasor transform for automatic delineation of single-lead ECG fiducial points

View the article online for updates and enhancements.

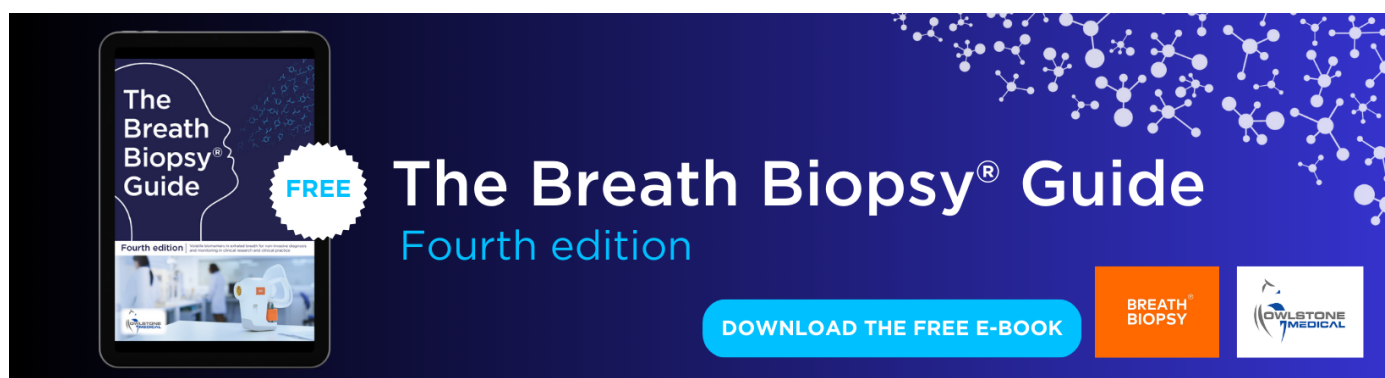# Application of the phasor transform for automatic delineation of single-lead ECG fiducial points

Arturo Martínez[1]**, Raúl Alcaraz**[1] **and José Joaquín Rieta**[2]

[1] Innovation in Bioengineering Research Group, University of Castilla La Mancha, Spain
[2] Biomedical Synergy, Electronic Engineering Department, Universidad Politécnica de Valencia, Spain

E-mail: arturo.martinez@uclm.es, raul.alcaraz@uclm.es and jjrieta@eln.upv.es

Abstract

This work introduces a new single-lead ECG delineator based on phasor transform. The method is characterized by its robustness, low computational cost and mathematical simplicity. It converts each instantaneous ECG sample into a phasor, and can precisely manage P and T waves, which are of notably lower amplitude than the QRS complex. The method has been validated making use of synthesized and real ECG sets, including the MIT-BIH arrhythmia, QT, European ST-T and TWA Challenge 2008 databases. Experiments with the synthesized recordings reported precise detection and delineation performances in a wide variety of ECGs, with signal-to-noise ratios of 10 dB and above. For real ECGs, the QRS detection was characterized by an average sensitivity of 99.81% and positive predictivity of 99.89%, for all the analyzed databases (more than one million beats). Regarding delineation, the maximum localization error between automatic and manual annotations was lower than 6 ms and its standard deviation was in agreement with the accepted tolerances for expert physicians in the onset and offset identification for QRS, P and T waves. Furthermore, after revising and reannotating some ECG recordings by expert cardiologists, the delineation error decreased notably, becoming lower than 3.5 ms, on average, and reducing by a half its standard deviation. This new proposed strategy outperforms the results provided by other well-known delineation algorithms and, moreover, presents a notably lower computational cost.

1. Introduction

The surface electrocardiogram (ECG) provides a widely used and comfortable way to study the heart function, being a conventional tool for the diagnosis of cardiac diseases, which are the main cause of mortality in our society (Sörnmo and Laguna 2005, Petrutiu *et al* 2006). Given that most of the clinically useful information in the ECG is found within the time intervals and amplitudes determined by its fiducial points, the development of accurate and robust methods for automatic ECG delineation is a very interesting challenge for clinicians and biomedical engineers (Martínez *et al* 2004). In this respect, precise ECG fiducial point detection could help in the achievement of more accurate results in applications such as pattern recognition or arrhythmia classification (Minhas and Arif 2008) and to develop improved solutions for the diagnosis of certain phenomena such as T-wave alternans (Ghaffari *et al* 2009), atrial fibrillation (Minhas and Arif 2008) or QT-prolongation (Christov and Simova 2007).

The lack of any universally accepted rule defining the ECG waves onset and offset has been an extra complication to systematize ECG waves delineation; however, many authors have addressed this issue. Thus, a wide diversity of algorithms have been proposed in the literature (Martínez *et al* 2004). Most of them work on a single ECG lead and relay, as a first step, on R-peak detection in order to take this point as a reference. The most significant proposed approaches to locate the R-peak are summarized in Köhler *et al* (2002). The next usual step is to delineate the QRS complex and, next, the P and T waves. In this respect, most of the algorithms usually start from the R-peak and define forward and backward seek windows. However, the precise detection of the wave onset and offset directly from the ECG is a hard task because, in general, the signal amplitude is notably low near the wave boundaries and the noise level can be even higher than the signal itself (Martínez *et al* 2004). Thereby, once the seek window is defined, some technique has to be applied to the ECG in order to enhance the proper waves and fiducial points. In this respect, different mathematical tools, including filters (Koeleman *et al* 1985, Soria-Olivas *et al* 1998), first-order (FD) and second-order derivatives (Arzeno *et al* 2008, Kemmelings *et al* 1994), low-pass differentiation (LPD) (Laguna *et al* 1994, Speranza *et al* 1993), nonlinear time-scale decomposition (Strumillo 2002), dynamic time warping (Vullings *et al* 1998), artificial neural networks (Dokur *et al* 1997), Hilbert Transform (HT) (Hickey *et al* 2004), hidden Markov models (Clavier *et al* 2002), etc, have been used. However, wavelet transform (WT) has proved to be the delineation method with the highest accuracy (Martínez *et al* 2004, Ghaffari *et al* 2009). Nevertheless, WT-based delineation algorithms require intensive mathematical operations and, therefore, notable computational time and cost (Patil and Abel 2009).

In the present contribution, an easy to implement and fast algorithm based on phasor transform (PT) is proposed to detect and delineate QRS, P and T waves from the ECG. The performance of this technique is assessed using synthesized ECGs and standard real ECG databases manually annotated, with which other algorithms have already been tested: MIT-BIT arrhythmia (Moody and Mark 1990), QT (Laguna *et al* 1997), European ST-T (Taddei *et al* 1992) and TWA Challenge 2008 (Moody 2008) comprise the real tested datasets.

The paper is structured as follows. Section 2 describes the proposed PT-based algorithm for detection and delineation of ECG waves together with its validation from synthetic and real ECG recordings. Section 3 summarizes the results obtained for the different analyzed databases. These outcomes are discussed and compared with others provided by well-known delineation methods in section 4. Finally, section 5 presents the concluding remarks bringing the paper to its end.
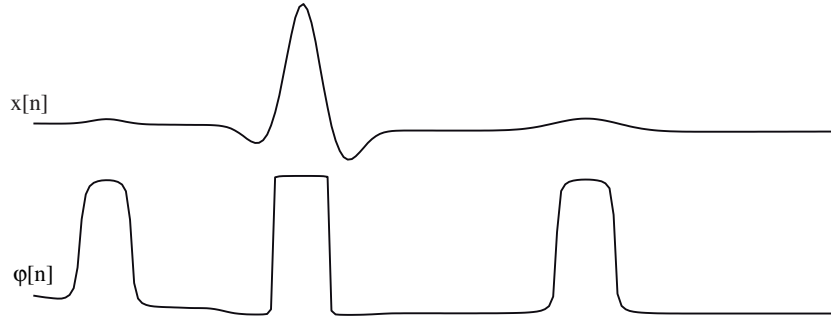
Figure 1. Example of an ECG beat, $x[n]$, with P and T waves of notably low amplitude together with the resulting phasor transformed signal, $\varphi[n]$, in which these waves are remarkably enhanced.

2. Methods

2.1. Phasorial signal for delineation

The PT is an easy tool that can represent a sinusoidal function in the complex domain. The result is a complex number, called phasor, which preserves the signal information regarding root mean square and phase values (Proakis and Manolakis 1996). Thus, for a generic discrete sinusoid such as

$$x[n] = A\cos(\omega n + \varphi) = \Re\{A\,e^{j(\omega n + \varphi)}\}, \tag{1}$$

A being the amplitude and φ the phase of the sinusoid, its PT would provide a rotating phasor in the complex plane with magnitude A, rotation speed ω and initial phase φ, i.e.

$$PT\{x[n]\} = A\,e^{j\varphi} = A\cos(\varphi) + jA\sin(\varphi). \tag{2}$$

To enhance the ECG waves, PT was used to convert each instantaneous ECG sample into a phasor. A constant value R_v was considered as the real part, whereas the original value of the ECG sample was used as the imaginary component of the phasor. Thus, if we denote an ECG recording of N samples in length by $x[n]$, n being the discrete time, the phasor $y[n]$ could be defined for each sample as

$$y[n] = R_v + jx[n], \qquad \text{for} \quad n = 1, \dots, N. \tag{3}$$

The magnitude $M[n]$ and phase $\varphi[n]$ of this phasor could be computed as

$$M[n] = \sqrt{R_v^2 + x[n]^2} \quad \text{and} \tag{4}$$

$$\varphi[n] = \tan^{-1}\left(\frac{x[n]}{R_v}\right). \tag{5}$$

In this way, by considering the instantaneous phase variation in consecutive samples of the phasor transformed ECG, the slight variations provoked by P and T waves in the original recording are maximized, regardless of their eventually low amplitude, such as can be observed in figure 1, thus making their detection and delineation notably easier.

The value of R_v determines the degree with which ECG waves are enhanced in the phasorial signal. Thus, the lower R_v, the higher the differences among phase variations in the complex plane. In this respect, for the limit case in which $R_v = 0$, the phase signal $\varphi[n]$ only presents two values:

$$\varphi[n] = \begin{cases} +\frac{\pi}{2} & \text{if} \quad x[n] \geqslant 0 \\ -\frac{\pi}{2} & \text{if} \quad x[n] < 0 \end{cases}. \tag{6}$$
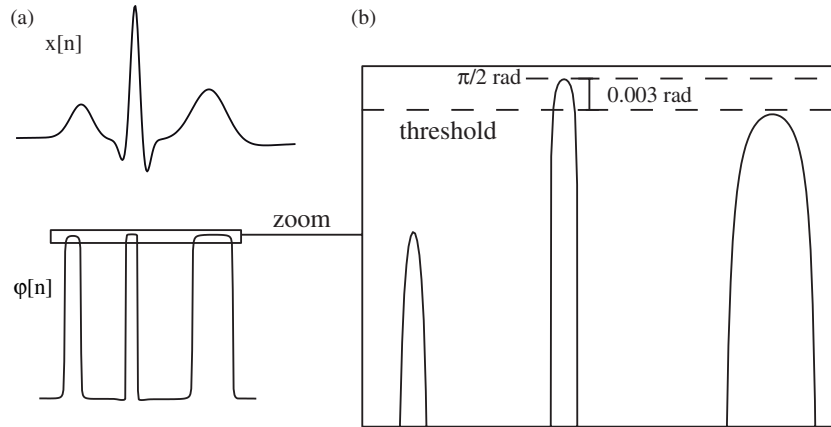
Figure 2. (a) Representation of a normal beat from a typical ECG (top) together with its phase variation obtained from the phasor transform (bottom). (b) Detailed representation of the phasor transformed signal $\varphi[n]$ to illustrate the process for R-peak identification.

For the opposite case, in which $R_v = 1$, the original ECG with a maximum amplitude of $\pi/4$ rad would be obtained, whenever the ECG would be normalized to its maximum R-peak amplitude.

2.2. Detection sequence of the fiducial points

2.2.1. QRS detection. QRS complexes were detected by directly applying the PT, with a value of $R_v = 0.001$, to the absolute value of the original ECG, $|x[n]|$, previously removing its baseline wander with forward/backward high-pass filtering of 0.5 Hz cut-off frequency. As can be seen in the lower panel of figure 2(a), P and T waves were notably enlarged by the PT operation. Anyway, the maximum instantaneous phase variation can yet be found for the QRS complex, as figure 2(b) shows. Thus, by establishing a threshold of 0.003 rad below the maximum phase variation ($\pi/2$), the QRS complexes can be located as those segments exceeding the threshold. Similarly, the R-peak of each beat can be marked as the maximum magnitude $M[n]$ point within each segment. In those cases where a time longer than 150% of the last computed R–R distance elapsed without detecting any QRS, a new backward seek with lowered thresholds was repeated until successful detection. On the contrary, when two R points were localized within an interval lower than 40% of the distance between the last two R peaks, the one with lower magnitude $M[n]$ was discarded to prevent double R detection within a beat.

2.2.2. QRS delineation. Once the R-peak was detected, it served as a reference for the identification of Q and S waves. Two boundary points, γ_{QRS-} and γ_{QRS+}, around the R-peak were primarily established. They were defined as the closer points to the R-peak in which $\varphi[n]$ was lower than 25% of the maximum phase variation ($\pi/2$). Before γ_{QRS-}, a window of 35 ms was considered to seek for the Q wave. Only for this window, the PT was newly applied to the absolute value of the ECG, $|x[n]|$, subtracting previously the median of the segment. In this case, the value of R_v was 0.005 in order to minimize the effect of interfering noise. Finally, the local minimum of $\varphi[n]$ was sought within the defined window. If any point presented a phase higher than 50% of the maximum variation within the window, the marked local minimum was annotated as the Q wave, given that the absence of a significant negative
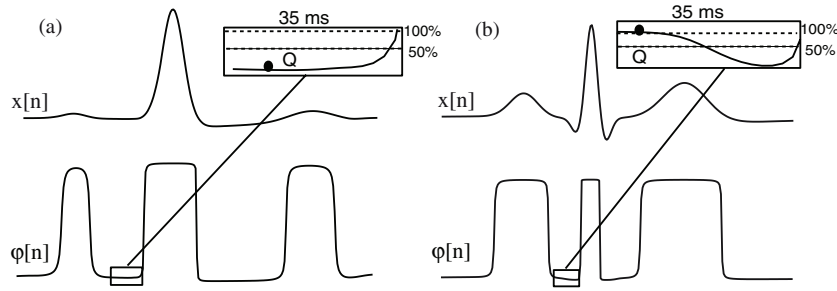
Figure 3. Example of a beat without (a) and with (b) negative deflection, with respect to the isoelectric line, between fiducial points Q and R and how the proposed method behaves.

deflection with respect to the isoelectric line between Q and R was deduced, see figure 3(a). In other case, among the phasors exceeding the threshold, the one with the highest magnitude $M[n]$ was marked as the Q wave, because this point will be the local minimum preceding the described deflection, see figure 3(b).

The definition of γ_{QRS-} allows an appropriate Q wave delineation in wide QRS complexes since the search window can be established accurately. On the contrary, if a fixed search window would be considered from the R-peak, such as in most previous works (Martínez *et al* 2004), the Q wave could not be located within the window, thus making the accurate delineation of the wave unfeasible under some scenarios (Arzeno *et al* 2008).

The same strategy and window length were used for S wave delineation, with the only particularity that the seek window was defined after the point γ_{QRS+}.

2.2.3. P wave detection and delineation.   In order to detect the P wave, a seek window, relative to the Q wave position, was considered. The width of this window was adapted to each beat, being initially a quarter of the distance between the current R-peak and the previous one. Afterward, the median was removed from the ECG segment within the window and PT was applied with R_v taking a value of 0.003. The local maximum of $\varphi[n]$ was located within the window and it corroborated the coherence of this point with a peak. For this purpose, it was checked that the preceding and subsequent samples presented a magnitude $M[n]$ lower than the marked point. In the affirmative case, the point was annotated as the maximum value of the P wave. In contrast, the width of the seek window has to be reduced because, eventually, some part of the T wave from the preceding beat could be considered within the initial window. Iteratively, the aforementioned process was repeated until the detection of the P wave peak. Finally, when the detected P wave amplitude was lower than 5% of the R-peak amplitude, an absence of the P wave was considered.

For identification of the P wave onset and offset, the detected P-peak served as a reference. Both boundaries were individually searched. Thus, a 15 ms window relative to the P-peak was established before this point. The median was removed and PT, with $R_v = 0.005$, was applied to the ECG segment within the window. Next, the first derivate of $\varphi[n]$ was obtained to locate the phase transition from its minimum to its maximum, see figure 4. Afterward, from this point toward the window start, the nearest zero-crossing in $\varphi'[n]$ was searched and marked as the P wave onset. The P wave offset detection was based on the same process, but with two differences. Obviously, the seek window was established after the P-peak and the closest zero-crossing in $\varphi'[n]$ was sought from its local minimum toward the window end. In those cases where the P wave onset or offset was not found after the aforementioned process,
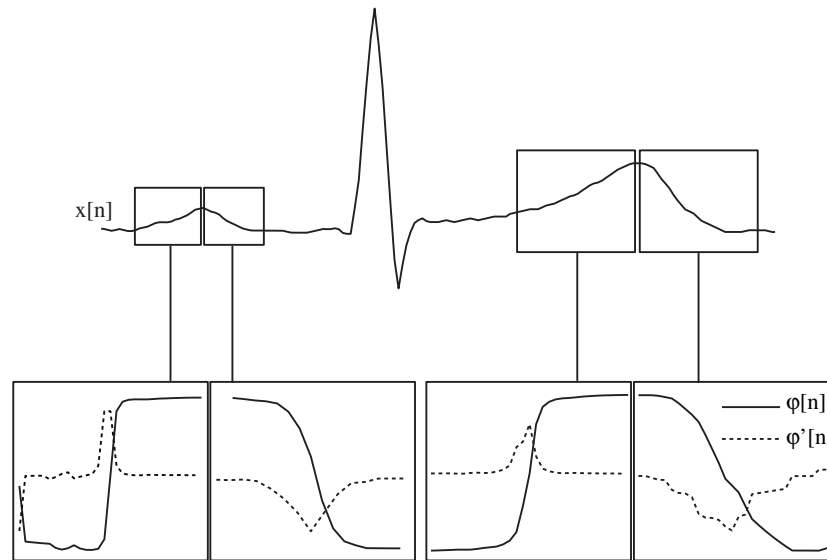
Figure 4. Representation of the phasorial signals, $\varphi[n]$, and their corresponding derivative, $\varphi'[n]$, used to delineate the onset and offset associated with P and T waves of the ECG beat.

the same approach would be repeated with a lower value of R_v until the location of both boundaries.

2.2.4. T wave detection and delineation. The strategy to identify the T wave peak and boundaries was similar to that described for the P wave. In this case, a wider seek window of 25 ms was used to determine the onset and offset of the T wave, because it is generally longer than the P wave. Additionally, given that the T wave amplitude is higher than the P wave, a lower enhancement of this wave was required and, therefore, a value of $R_v = 0.1$ was used as PT computational parameters.

2.3. Validation of the delineator

Given the lack of a *gold standard* to determine ECG fiducial points, the proposed delineator was validated making use of manually annotated databases. Thus, in order to evaluate the robustness of the algorithm against random noise, a database with synthetic ECG recordings annotated by expert cardiologists was used first. Afterward, the algorithm was assessed making use of easily available databases of real ECGs, which has been widely used for validation in previous works (Martínez *et al* 2004, Ghaffari *et al* 2009).

2.3.1. Synthetic ECG database. Fifty 30 s synthetic ECG signals were generated making use of a previously published algorithm (McSharry *et al* 2003) with a sampling frequency of 250 Hz. The most typical morphologies for QRS complexes (QRS, RSR', RS, R and QS), P wave (positive, negative, biphasic and absent) and T wave (positive, negative, biphasic and absent) were considered and randomly distributed throughout the signals, as figure 5 shows. To obtain realistic ECG waveforms, the amplitude of each wave was modulated, in a beat-to-beat basis, being divided by a random factor between 1 and 2.5, thus achieving an attenuation between 0% and 60% of its original value (Sörnmo and Laguna 2005). In addition, the distance
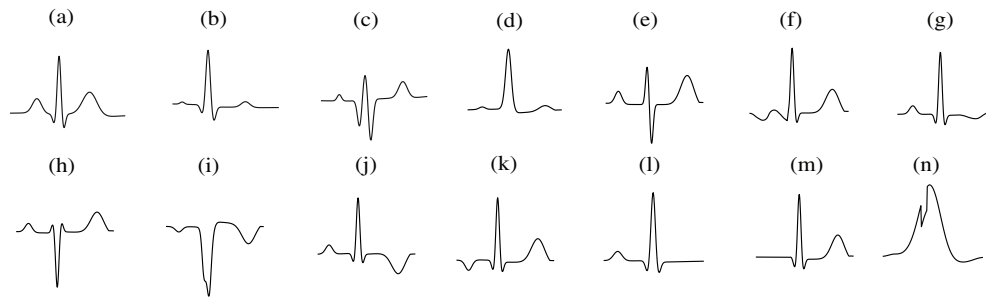
Figure 5. Different morphologies of QRS, P and T waves included in the synthetic signals set: (a) normal QRS, P and T waves, (b) normal QRS and attenuated P and T waves, (c) attenuated normal QRS with normal P and T waves, (d) R complex with attenuated P and T waves, (e) RS complex with normal P and T waves, (f) normal QRS and T waves with biphasic P, (g) normal QRS and P waves with biphasic T, (h) RSR' complex with normal P and T waves, (i) QS complex with negative P and T waves, (j) normal QRS and P waves with negative T, (k) normal QRS and T waves with negative P, (l) normal QRS and P waves without T, (m) normal QRS and T waves without P, and (n) premature ectopic ventricular contraction.

between consecutive R peaks was also varied within an interval of $\pm30\%$ of the mean heart rhythm, which was randomly selected between 60 and 140 beats min^{-1} for each synthesized recording.

The generated recordings were manually annotated by expert cardiologists from a digital support in order to avoid possible digitalization errors in the annotations. It should be noted that the parameters of the proposed delineation algorithm were fixed, making use of this database as a training set. Afterward, different levels of random noise were added to the synthetic signals to analyze the robustness of the delineator. Precisely, signal-to-noise ratios (SNR) of 40, 30, 20 and 10 dB were studied, given that the SNR of a typical ECG recording ranges from 10 to 40 dB (Yu and Chen 2009). The delineator was applied to these noisy signals and its performance was assessed for comparison with the initial annotations. In this respect, the detection of each analyzed point was evaluated by computing the sensitivity, $\text{Se} = \text{TP}/(\text{TP} + \text{FN})$, the positive predictivity, $P^+ = \text{TP}/(\text{TP} + \text{FP})$, and the failed detection percentage, $F_d = (\text{FP} + \text{FN})/\text{TB}$, TP being the number of true positives, FP the number of false positives, FN the number of false negatives and TB the number of analyzed beats. The location error (LE) was computed from the differences between manual and automatic annotations in order to validate the wave delineation accuracy.

2.3.2. Real ECG database. Several databases with different sampling frequencies (f_s) and SNRs were used to validate the proposed delineator performance from real ECGs. The MIT-BIH arrhythmia database (MITDB), the QT database (QTDB), the European ST-T database (EDB) and the TWA Challenge 2008 database (TWADB) were enrolled in the study. Their main characteristics are summarized in table 1.

The MITDB includes mainly selected Holter recordings with anomalous but clinically important phenomena. This database presents annotations of the R-peak position. The EDB files contain ischemic episodes extracted from Holter signals with annotations of the QRS placement. The QTDB includes some recordings from EDB and MITDB and also from several other MIT-BITH databases (ST change, supraventricular arrhythmia, normal sinus rhythm, sudden death and long term). This database was developed for wave limit validation purposes with more than 3600 annotated beats. More precisely, it provides annotations,

Table 1. Characteristics of the real ECG databases used for validation in this work.

Database	Files	Leads	f_s (Hz)	Resol.	Rec. duration
MITDB	48	2	360	5 μV	30 min
QTDB	105	2	250	5 μV	15 min
EDB	90	2	250	5 μV	120 min
TWADB	100	2–12	500	5 μV	2 min

by an expert cardiologist, for at least 30 beats per recording, with marks including QRS complexes, P and T wave peaks, onsets and offsets. Additionally, in 79 out of 105 recordings, manually annotated QRS positions are provided for the whole signal. Finally, the TWADB contains annotations of R-peak positions for recordings obtained from patients with myocardial infarctions, transient ischemia, ventricular tachyarrhythmias and other risk factors for sudden cardiac death, as well as healthy controls and synthetic cases with calibrated amounts of T-wave alternants.

The QRS detection stage was validated making use of the four databases. R-peaks were only detected in the first lead of each recording in order to compare the obtained results with other published works. As for synthetic ECG signals, sensitivity, positive predictivity and failed detection percentage were computed to quantify the algorithm performance.

Regarding the delineation assessment of the proposed method, only the QTDB was used. Although the delineator works on a single-channel basis, it has to be remarked that annotations on the QTDB were performed having the two available leads in sight (Laguna *et al* 1997). This aspect could explain why a LE standard deviation higher than the tolerances recommended by the Common Standards of Electrocardiography (CSE) working party (CSE 1985) was noticed for several QTDB recordings. Thus, after revising the first channel of these recordings by expert cardiologists, notable differences between the original manual annotations and the recorded fiducial points were observed in several signals, as figure 6 shows for some of them. Thereby, expert cardiologists re-annotated the first channel of these recordings following a set of single-lead criteria. Next, the performance of the delineator was assessed again taking into consideration the new annotations, in a similar way to previous works (Ghaffari *et al* 2009 2010).

3. Results

Sensitivity and positive predictivity values of 100% and a LE of 0 ms were obtained in detection and delineation over synthesized ECGs without noise (SNR $= \infty$ dB), see table 2. This result has to be considered as not outstanding, given that the delineator was trained using these recordings. For the remaining SNRs, random noise was generated 100 times and added back to the synthesized ECG signals. Hence, the method's performance, both for detection and delineation, was assessed for the 100 noise realizations. The obtained mean values are also presented in table 2. As can be seen, the sensitivity and positive predictivity for detection of all the ECG waves were 100% for SNRs $\geqslant$ 20 dB and slightly lower for a SNR of 10 dB. Similar behavior can be observed for delineation, becoming the LE standard deviation higher than the accepted two standard deviation ($2\sigma_{CSE}$) tolerances, recommended by the CSE working party (CSE 1985), for the P wave onset and offset and the QRS onset, when the SNR was 10 dB.

The QRS detection performances on the MITDB, QTDB, EDB and TWADB obtained by the proposed algorithm and other previous single-lead methods are presented in tables 3–6.

Figure 6. Examples of QTDB recordings with remarkable differences between manual annotations, performed on a multi-lead basis, and the fiducial points recorded in the lead. The plotted ECG segments belong to (a) *sel102*, (b) *sel308*, (c) *sel104* and (d) *sel213* recordings. Re-annotations performed by expert cardiologists based on single-lead criteria are also shown.

Most of the previous detectors were tested on the MITDB (Ghaffari *et al* 2009, Martínez *et al* 2004, Li *et al* 1995, Moody and Mark 1982, Pan and Tompkins 1985, Hamilton and Tompkins 1986, Hickey *et al* 2004), although a few of them were also checked on the QTDB, EDB (Ghaffari *et al* 2009, Martínez *et al* 2004) and TWADB (Ghaffari *et al* 2009). Considering that in the most significant single-lead detectors presented to date (Martínez *et al* 2004, Ghaffari *et al* 2009) the segments with ventricular flutter in record 207 of the MITDB and those others annotated as unreadable in the EDB were excluded, we also followed the same procedure to validate the proposed algorithm. The obtained results are presented in

Table 2. Detection and delineation performance achieved by the proposed delineator when tested over the synthesized ECG database.

| Boundaries | TB | Parameters | SNR | | | | | $2\sigma_{CSE}$(ms) |
			∞ dB	40 dB	30dB	20dB	10 dB	
P_{on}	225 200	Se (%)	100	100	100	100	99.41	
		P^+(%)	100	100	100	100	93.18	
		LE ($\mu \pm \sigma$)(ms)	0 ± 0	2.8 ± 7.1	3.4 ± 10	4.1 ± 14.2	4.5 ± 38.5	10.2
P_{peak}	225 200	Se (%)	100	100	100	100	99.41	
		P^+(%)	100	100	100	100	93.18	
		LE ($\mu \pm \sigma$)(ms)	0 ± 0	-0.8 ± 2.7	1.9 ± 4.4	4.2 ± 9.0	6.1 ± 33	–
P_{end}	225 200	Se (%)	100	100	100	100	99.41	
		P^+(%)	100	100	100	100	93.18	
		LE ($\mu \pm \sigma$)(ms)	0 ± 0	3.0 ± 7.1	5.9 ± 9.3	6.5 ± 14.0	7.8 ± 42.9	12.7
QRS_{on}	225 200	Se (%)	100	100	100	100	100	
		P^+(%)	100	100	100	100	100	
		LE ($\mu \pm \sigma$)(ms)	0 ± 0	-3.1 ± 4.1	4.7 ± 4.7	5.9 ± 6.8	5.3 ± 12.0	6.5
R	225 200	Se (%)	100	100	100	100	100	
		P^+(%)	100	100	100	100	100	
		LE ($\mu \pm \sigma$)(ms)	0 ± 0	0.04 ± 0.2	0.2 ± 0.8	0.5 ± 2.1	0.6 ± 3.5	–
QRS_{end}	225 200	Se (%)	100	100	100	100	100	
		P^+(%)	100	100	100	100	100	
		LE ($\mu \pm \sigma$)(ms)	0 ± 0	0.9 ± 1.6	0.92 ± 2.2	-0.11 ± 3.7	0.47 ± 7.5	11.6
T_{on}	225 200	Se (%)	100	100	100	100	99.48	
		P^+(%)	100	100	100	100	95.45	
		LE ($\mu \pm \sigma$)(ms)	0 ± 0	1.6 ± 3.9	2.4 ± 9.2	14.5 ± 17.2	23.2 ± 25.4	–
T_{peak}	225 200	Se (%)	100	100	100	100	99.48	
		P^+(%)	100	100	100	100	95.45	
		LE ($\mu \pm \sigma$)(ms)	0 ± 0	0.7 ± 3.4	-0.8 ± 5.6	0.7 ± 9.8	1.30 ± 17.8	–
T_{end}	225 200	Se (%)	100	100	100	100	99.48	
		P^+(%)	100	100	100	100	95.45	
		LE ($\mu \pm \sigma$)(ms)	0 ± 0	1.4 ± 3.4	5.84 ± 9.6	13.9 ± 20.2	20.2 ± 26.4	30.6

the first row of tables 3–6. Moreover, recording 58 of the TWADB was not included in the analysis, because most parts of its P and T waves were masked by muscle noise, which is very difficult to remove. Nonetheless, note that there exists a standard protocol, specified in ANSI/AAMI EC57 (ANSI/AAMI-EC57 1998/(R)2008/(R), for meaningful performance comparison between QRS detection algorithms. Thus, to facilitate comparison with other detectors, the performance has also been assessed following the aforementioned protocol for the MITDB, QTDB and EDB databases. Results are presented in the second row of tables 3–5. In this case, segments with ventricular flutter in record 207 of the MITDB were also excluded, but those annotated as unreadable in the EDB were considered in the study. Furthermore, the

Table 3. Performance comparison of several QRS detection algorithms: application to MITDB (N/R: not reported).

Detection algorithm	TB	TP	FP	FN	$F_d(\%)$	Se(%)	$P^+(\%)$
PT (this work)	109 428	109 111	35	317	0.32	99.71	99.97
PT following the protocol ANSI/AAMI EC57	84 164	83 885	32	259	0.34	99.69	99.96
Ghaffari *et al* (2009)	109 428	109 327	129	101	0.21	99.91	99.88
Martínez *et al* (2004)	109 428	109 208	153	220	0.34	99.80	99.88
Hickey *et al* (2004)	N/R	N/R	N/R	N/R	N/R	98.50	98.40
Li *et al* (1995)	104 182[a]	104 070	65	112	0.17	99.89	99.94
Hamilton and Tompkins (1986)	109 267	108 927	248	340	0.54	99.69	99.77
Pan and Tompkins (1985)	109 809[a]	109 532	507	277	0.71	99.75	99.54
Moody and Mark (1982)	N/R	N/R	212	241	N/R	99.77	99.81

[a] Values computed according to the record-by-record tables in the referred works.

Table 4. Performance comparison of several QRS detection algorithms: application to QTDB.

Detection algorithm	TB	TP	FP	FN	$F_d(\%)$	Se(%)	$P^+(\%)$
PT (this work)	86 892	86 852	55	40	0.11	99.95	99.93
PT following the protocol ANSI/AAMI EC57	57 773	57 745	43	28	0.12	99.95	99.92
Ghaffari *et al* (2009)	86 892	86 845	79	47	0.15	99.94	99.91
Martínez *et al* (2004)	86 892	86 824	107	68	0.20	99.92	99.88

Table 5. Performance comparison of several QRS detection algorithms: application to EDB.

Detection algorithm	TB	TP	FP	FN	$F_d(\%)$	Se(%)	$P^+(\%)$
PT (this work)	787 103	784 515	2054	2588	0.59	99.67	99.73
PT following the protocol ANSI/AAMI EC57	759 878	757 280	2087	2598	0.61	99.66	99.72
Ghaffari *et al* (2009)	787 103	784 210	3554	2893	0.82	99.63	99.55
Martínez *et al* (2004)	787 103	784 059	4077	3044	0.90	99.61	99.48

Table 6. Performance comparison of two QRS detection algorithms: application to TWADB.

Detection algorithm	TB	TP	FP	FN	$F_d(\%)$	Se(%)	$P^+(\%)$
PT (this work)	18 847	18 830	16	17	0.17	99.90	99.91
Ghaffari *et al* (2009)	11 789	11 776	18	13	0.26	99.89	99.84

first 5 min of each recording was excluded and MITDB signals 102, 104, 107 and 217 were also not considered, because they contain poorly recorded paced beats. It should be noted that the aforementioned protocol cannot be applied to the TWADB, provided that its recordings are shorter than 5 min.

Table 7. Delineation performance comparison with the most significant previous works making use of the QT database (N/A: not applicable, N/R: not reported, LE: location error).

| Method	Parameters	P_{on}	P_{peak}	P_{end}	QRS_{on}	QRS_{end}	T_{peak}	T_{end}
PT on re-annotated QTDB	Se (%)	99.27	99.27	99.27	99.91	99.91	99.77	99.77
	P^+(%)	98.75	98.75	98.75	99.94	99.94	99.66	99.66
	LE ($\mu \pm \sigma$)(ms)	-3.2 ± 7.7	1.1 ± 2.0	-0.2 ± 3.5	-1.6 ± 3.3	-2.8 ± 4.0	0.46 ± 2.8	-2.5 ± 6.2
PT on originally annotated QTDB	Se (%)	98.65	98.65	98.65	99.85	99.85	99.20	99.20
	P^+(%)	97.52	97.52	97.52	99.72	99.72	99.01	99.01
	LE ($\mu \pm \sigma$)(ms)	2.6 ± 14.5	32 ± 25.7	0.7 ± 14.7	-0.2 ± 7.2	2.5 ± 8.9	5.3 ± 12.9	5.8 ± 22.7
Ghaffari *et al* (2009)	Se (%)	99.46	99.46	99.46	99.94	99.94	99.87	99.87
	P^+(%)	98.83	98.83	98.83	99.91	99.91	99.80	99.80
	LE ($\mu \pm \sigma$)(ms)	-1.2 ± 6.3	4.1 ± 10.5	0.7 ± 6.8	-0.6 ± 8	0.3 ± 8.8	0.3 ± 4.1	0.8 ± 10.7
Martínez *et al* (2004)	Se (%)	98.87	99.87	98.75	99.97	99.97	99.77	99.77
	P^+(%)	91.03	91.03	91.03	N/A	NA	97.79	97.79
	LE($\mu \pm \sigma$)(ms)	2.0 ± 14.8	3.6 ± 13.2	1.9 ± 12.8	4.6 ± 7.7	0.8 ± 8.7	0.2 ± 13.9	-1.6 ± 18.1
Laguna *et al* (1994)	Se (%)	97.7	97.7	97.7	99.92	99.92	99.0	99.0
	P^+(%)	91.17	91.17	91.17	N/A	NA	97.74	97.71
	LE($\mu \pm \sigma$)(ms)	14.0 ± 13.3	4.8 ± 10.6	-0.1 ± 12.3	-3.6 ± 8.6	-1.1 ± 8.3	-7.2 ± 14.3	13.5 ± 27.0
Vila *et al* (2000)	Se (%)	N/A	N/A	N/A	N/A	N/A	92.6	92.6
	P^+(%)	N/A	N/A	N/A	N/A	N/A	N/R	N/R
	LE($\mu \pm \sigma$)(ms)	N/A	N/A	N/A	N/A	N/A	-12 ± 23.4	0.8 ± 30.3
Tolerances $2\sigma_{CSE}(ms)$		10.2	–	12.7	6.5	11.6	–	30.6

Finally, with regard to delineation, table 7 shows a comparison of the results between the proposed delineator and other methods (Martínez *et al* 2004, Ghaffari *et al* 2009, Laguna *et al* 1994, Vila *et al* 2000) when analyzing the QT database.

4. Discussion

4.1. Synthetic ECG recordings

Regarding QRS detection, results with synthetic ECG signals showed that R-peaks were robustly localized by the proposed algorithm since sensitivity and positive predictivity presented values of 100%, even with notably high noise levels (SNR of 10 dB), see table 2. This good outcome proves that the method is able to correctly detect the QRS complex independently of its morphology, given that the synthesized database included a wide variety of the most common cases. A similar observation could be made for P and T waves in which, for all the synthesized different morphologies, sensitivity and positive predictivity were higher than 99.41% and 93.18%, respectively (see table 2).

For the T wave offset delineation, a considerably reduced LE was observed for all the SNRs, its standard deviation being lower than the accepted CSE tolerance (CSE 1985), even for SNRs of 10 dB, see table 2. Similar behavior was also observed for the QRS offset delineation.
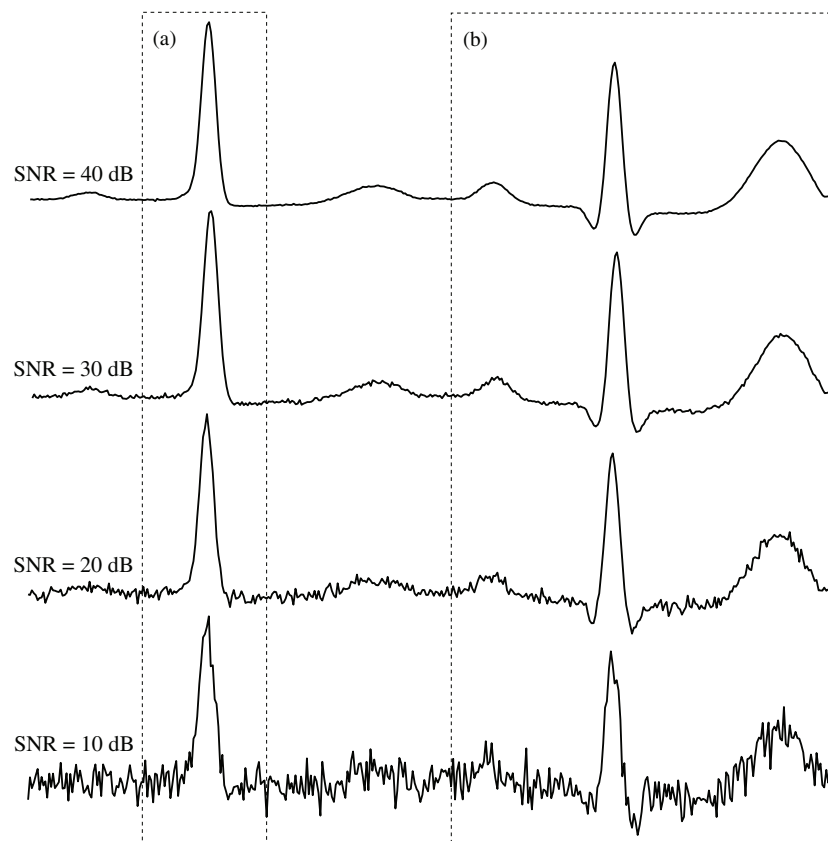
Figure 7. Representation of a synthetically generated (a) R complex and (b) normal beat with different noise levels. It can be seen that Q and P waves are disfigured and finally disappeared as noise increases.

However, for the QRS onset, the LE standard deviation was higher than the accepted CSE tolerance for an SNR $\leqslant$ 20 dB. The fact that the Q wave can be easily masked by the noise when there is no significant negative deflection between Q and R points, as figure 7(a) shows, could be a possible justification of this result. With regard to the P wave edges delineation, a higher LE standard deviation than the accepted CSE tolerances was also observed for an SNR $\leqslant$ 20 dB. In this case, a possible reason could be that the P wave is notably disfigured and finally masked by the noise corresponding to SNRs of 20 and 10 dB, respectively, such as can be seen in figure 7(b). Overall, it could be considered that the proposed algorithm is able to correctly delineate T waves from ECGs with SNRs higher than 10 dB and QRS complexes and P waves from recordings with an SNR > 20 dB.

4.2. QRS detection with real ECGs

By averaging the results provided by the four analyzed real ECG databases, the proposed method achieved a sensitivity of 99.81% and a positive predictivity of 99.89% in QRS detection. In this case, the databases were evaluated following the procedure described in

the most significant single-lead delineators presented to date (Martínez *et al* 2004, Ghaffari *et al* 2009), which did not follow the standard protocol ANSI/AAMI EC57. When the protocol was followed, the obtained results were almost the same, given that, on average, sensitivity was 99.77% and positive predictivity was 99.87%. Thus, in the worst case, failed detection percentage was only increased by 0.02%, and sensitivity and positive predictivity were only reduced by 0.02% and 0.01%, respectively. Regardless of protocol ANSI/AAMI EC57, in both experiments one million beats with different morphologies were used, approximately, to validate the detector. The obtained outcomes were equal or slightly better than those reported by the aforementioned single-lead delineation algorithms, i.e. Ghaffari *et al* (2009) ($Se =$ 99.84% and $P^+ = 99.80\%$) and Martínez *et al* (2004) ($Se = 99.66\%$ and $P^+ = 99.56\%$). Additionally, it should be noted that the proposed method was only trained making use of the synthetic ECG database. Hence, the detector parameters were not tuned to any of the real ECG used sets. In contrast, in the two aforementioned previous works (Ghaffari *et al* 2009, Martínez *et al* 2004), the MITDB was simultaneously used as the training and test set, which could imply an over-improvement of the real outcomes for this database.

The MITDB is characterized by a high density of premature ventricular contractions. The notably high amplitude of these ectopic beats in comparison with normal complexes complicates a reliable detection of all the R-peaks existing in the ECG by using thresholding (Arzeno *et al* 2008). Thus, to improve the QRS detection, more than one threshold and complex decision rules are normally required, such as several previous works have reported (Ghaffari *et al* 2009, Martínez *et al* 2004, Hickey *et al* 2004, Li *et al* 1995, Hamilton and Tompkins 1986, Pan and Tompkins 1985, Moody and Mark 1982). However, the proposed algorithm in this work only requires a threshold to reliably detect the R-peaks, given that the PT application to normal and ectopic beats, independently of their amplitude, produces a very similar phase variation, such as can be observed in figure 8. Obviously, this advantage is a valuable aid in the arduous detection of low-amplitude QRS complexes, as figure 9 shows. This fact could be the reason why the proposed method attains a performance on the MITDB, see table 3, slightly better than the one presented by the FD-based (Hamilton and Tompkins 1986, Pan and Tompkins 1985, Moody and Mark 1982) and HT-based (Hickey *et al* 2004) techniques, which use two thresholds, and very similar to those others reported by the WT-based methods (Ghaffari *et al* 2009, Martínez *et al* 2004, Li *et al* 1995), which make use of several thresholds and complex decision rules, thus notably increasing the computational burden.

As mentioned in section 2.2.1, the proposed method prevents the detection of two R-peaks within a beat. This fact is essential to reduce the number of false positives provoked by high and narrow T waves, which have been found to be a problem in methods in which R-peak detection relies on automatic thresholding (Martínez *et al* 2004, Ghaffari *et al* 2009, Li *et al* 1995, Pan and Tompkins 1985, Moody and Mark 1982, Hamilton and Tompkins 1986). As an example, in Martínez *et al* (2004), only the signal *e0305* of the EDB, which presents the described T wave morphology, provoked the 42% of the FP and the 57% of the FN reported for the whole database. On the contrary, for the PT-based method, this recording only provoked 0.58% of the FP and 3.79% of the FN obtained in the EDB. This could be the reason why the proposed algorithm presented the best sensitivity and positive predictivity for the European ST-T database in comparison with the works published to date, see table 5.

Regarding the QRS detection on the QTDB and TWADB, slightly better results were obtained with the proposed method than with other R-peak detectors, as can be seen in tables 4 and 6. In addition, it is noteworthy that the proposed algorithm was validated with a higher number of beats than the one used in previous works for the TWADB (Ghaffari *et al* 2009). Specifically, 59.87% of additional beats have been used in this study.
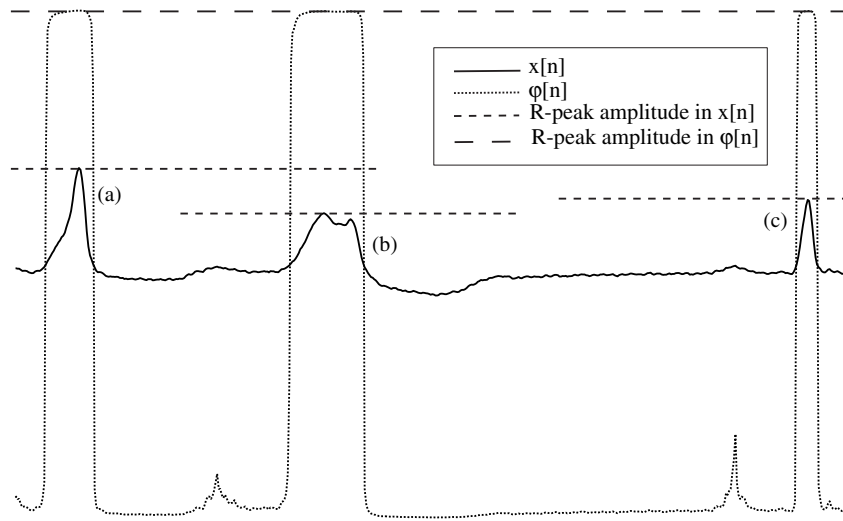
Figure 8. ECG segment extracted from recording 208 of the MITDB in which the application of the PT to (a) a ventricular ectopic, (b) a wide QRS and (c) a normal beat can be visualized. It can be seen that the amplitude differences in the ECG among beats disappear in the phasor transformed signal, $\varphi[n]$.
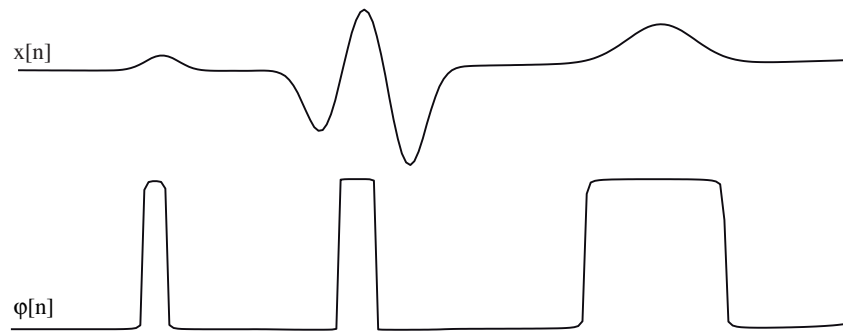
Figure 9. Representation of an ECG, $x[n]$, with a low-amplitude QRS complex, compared with the P and T waves, in which direct R-peak detection could be arduous by thresholding. Result of the phase transformed signal, $\varphi[n]$, in which QRS detection is made easier.

4.3. Wave delineation with real ECGs

The delineation performance on the QTDB demonstrated that the proposed delineator was able to detect the edges of the QRS, P and T waves with sensitivity and positive predictivity higher than 98.60% and 97.52%, respectively, see table 7. In addition, the algorithm identified the onset and offset of the P and QRS waves with mean localization errors smaller than one sample (4 ms). These results are very similar to previous works also based on single-lead delineators (Martínez *et al* 2004). For the T wave offset delineation, a mean difference between automatic and manual annotations slightly higher than one sample (around 5.8 ms) was observed. This result was similar to the one presented in Martínez *et al* (2004), if we consider the sampling time interval. Moreover, it should be remarked that identification of this point is the most

difficult task in ECG delineation, because a specific criterium to mark the T wave offset has not yet been adopted by specialists (Martínez *et al* 2004). Indeed, T wave offset annotations by different cardiologists on the same ECGs generally show larger differences (Martínez *et al* 2004).

Several previous works have considered the values given by the CSE Working Party (CSE 1985) as the limits that should not exceed the LE standard deviation for an appropriate ECG delineation. However, two interpretations of these tolerances can be found in the literature. Thus, some authors considered as strict limits (strict criterion) the standard deviation values recommended by CSE (σ_{CSE}) (de Chazal and Celler 1996, Strumillo 2002), while others took double these values ($2 \cdot \sigma_{CSE}$) as tolerances (loose criterion) (Ghaffari *et al* 2009, Martínez *et al* 2004, Vila *et al* 2000, Laguna *et al* 1994, Sahambi *et al* 1997, Vullings *et al* 1998). In this respect, the proposed delineation algorithm accomplished the loose criterion in QRS and T offsets, and nearly for the P onset and offset and the QRS onset, in a similar way to Martínez *et al*'s single-lead delineator (Martínez *et al* 2004). To our knowledge, only the most recently published single-lead delineator (Ghaffari *et al* 2009) currently accomplishes the strict criterion for the T wave offset identification and nearly for P onset and offset and QRS offset. However, annotations for challenging cases were revised and re-annotated by specialists prior to the method's validation (Ghaffari *et al* 2009). In a similar way, after re-annotating the first channel of some QTDB recordings with a set of single-lead criteria, the proposed algorithm provided a notably reduced LE for delineation of all the wave edges, accomplishing the strict criterion of the CSE recommendations for the P and T wave offsets and the QRS onset and offset, and nearly for the P onset. Additionally, the LE for the P and T peaks delineation was drastically reduced to be lower than 1.2 ms, thus making the PT-based delineator results better than the ones reported in Ghaffari *et al* (2009), except for the P wave onset.

The agreement between this study and Ghaffari *et al*'s work (Ghaffari *et al* 2009), regarding the achievement of better delineation results when some QTDB recordings were re-annotated following a single-lead basis, leads us to suggest that the validation of any single-channel algorithm should be carried out making use of databases annotated in only one lead. In this way, a more effective assessment and comparison between algorithms could be obtained, such as other authors have also highlighted in previous works (Martínez *et al* 2004). However, it should be noted that the time-variant electrical activity of the heart is reflected on each ECG lead within different time instants which, eventually, could impair accurate identification of the onset and end of the cardiac phenomena from only one lead (Almeida *et al* 2009). Nevertheless, the multi-lead algorithms presented to date have only marginally outperformed the delineation accuracy achieved by single-lead methods (Almeida *et al* 2009, Ghaffari *et al* 2010). Additionally, these multi-lead methods are based on a single-lead algorithm which, later, makes some decision about which lead has to be selected at any time. This fact notably increases their computational burden and/or complexity with no dramatical improvement. In this respect, some methods combine information obtained from the single-channel delineation of each available lead to provide a global identification of the cardiac events. Others apply an approach, previously performed over a single-channel delineation, to the signal obtained from the transformation of several leads in order to exploit their spatial information (Almeida *et al* 2009, Ghaffari *et al* 2010). As a consequence, the development of a single-lead delineator can be considered as the natural first step which is introduced in this work. Nonetheless, the information provided by the present algorithm, when applied over each available ECG lead, could be combined to deliver multi-channel delineation. However, this is not a trivial task and requires future investigations in the development of robust decision rules.

5. Conclusions

An innovative method for detection and delineation of single-lead ECG fiducial points has been presented. The phasor transform-based algorithm is characterized by its robustness, low computational cost, mathematical simplicity and ability to properly delineate the most typical morphologies of QRS, P and T waves. Furthermore, the method is able to delineate without requiring specific rules adapted to each specific ECG wave, whenever the SNR of the recording is higher than 10 dB. Thus, the method has proved to be a reliable and accurate delineator of real ECGs, slightly outperforming other previously published algorithms. Results with manual re-annotation suggest that the use of databases with single-channel annotations would allow a more effective assessment of new single-lead methods and comparison among them.

Acknowledgments

Appendix A. Table of symbols and abbreviations

Symbol or abbreviation	Description
CSE	Common standards of electrocardiography
EDB	European ST-T database
ECG	Electrocardiogram
FD	First derivative
FN	False negative
FP	False positive
F_s	Sampling frequency
HT	Hilbert transform
LE	Location error
LPD	Low-pass differentiation
MITDB	MIT-BIH arrhythmia database
N/R	Not reported
N/A	Not applicable
PT	Phasor transform
$P+$	Positive predictivity
P_{on}	P wave beginning
P_{peak}	P wave peak
P_{end}	P wave ending
QTDB	QT database
QRS_{on}	QRS wave beginning
R	R peak
QRS_{end}	QRS wave ending

Symbol or abbreviation	Description
Se	Sensitivity
SNR	Signal-to-noise ratio
TB	Total beats
TP	True positive
TWADB	T-Wave Alternans Challenge Database
T_{on}	T wave beginning
T_{peak}	T wave peak
T_{end}	T wave ending
WT	Wavelet transform
$M[n]$	Magnitude
$x[n]$	Original signal
$\phi[n]$	Phase
$\phi'[n]$	Phase's Derivative
Rv	Enhancement variable
γ_{QRS-}	Fiducial point for Q wave delineation
γ_{QRS+}	Fiducial point for S wave delineation
μ	Mean
σ	Standard deviation

References

Almeida R, Martínez J P, Rocha A P and Laguna P 2009 Multilead ECG delineation using spatially projected leads from wavelet transform loops *IEEE Trans. Biomed. Eng.* **56** 1996–2005

ANSI/AAMI-EC57 1998/(R)2008 Testing and reporting performance results of cardiac rhythm and ST segment measurement algorithms

Arzeno N M, Deng Z-D and Poon C-S 2008 Analysis of first-derivative based QRS detection algorithms *IEEE Trans. Biomed. Eng.* **55** 478–84

Christov I and Simova I 2007 Q-onset and T-end delineation: assessment of the performance of an automated method with the use of a reference database *Physiol. Meas.* **28** 213–21

Clavier L, Boucher J M, Lepage R, Blanc J J and Cornily J C 2002 Automatic P-wave analysis of patients prone to atrial fibrillation *Med. Biol. Eng. Comput.* **40** 63–71

CSE 1985 Recommendations for measurement standards in quantitative electrocardiography. The CSE Working Party *Eur. Heart. J.* **6** 815–25

de Chazal P and Celler B 1996 Automatic measurements of the QRS onset and offset in individual ECG leads *Conf. IEEE Eng. Med. Biol. Soc.* **4** 1399–400

Dokur Z, Olmez T, Yazgan E and Ersoy O K 1997 Detection of ECG waveforms by neural networks *Med. Eng. Phys.* **19** 738–41

Ghaffari A, Homaeinezhad M R, Akraminia M, Atarod M and Daevaeiha M 2009 A robust wavelet-based multi-lead electrocardiogram delineation algorithm *Med. Eng. Phys.* **31** 1219–27

Ghaffari A, Homaeinezhad M R, Khazraee M and Daevaeiha M M 2010 Segmentation of holter ECG waves via analysis of a discrete wavelet-derived multiple skewness-kurtosis based metric *Ann. Biomed. Eng.* **38** 1497–510

Hamilton P S and Tompkins W J 1986 Quantitative investigation of QRS detection rules using the MIT/BIH arrhythmia database *IEEE Trans. Biomed. Eng.* **33** 1157–65

Hickey B, Heneghan C and de Chazal P 2004 Non-episode dependent assessment of paroxysmal atrial fibrillation through measurement of RR interval dynamics and atrial premature contractions *Ann. Biomed. Eng.* **32** 677–87

Kemmelings J G, Linnenbank A C, Muilwijk S L, SippensGroenewegen A, Peper A and Grimbergen C A 1994 Automatic QRS onset and offset detection for body surface QRS integral mapping of ventricular tachycardia *IEEE Trans. Biomed. Eng.* **41** 830–6

Koeleman A S, Ros H H and van den Akker T J 1985 Beat-to-beat interval measurement in the electrocardiogram *Med. Biol. Eng. Comput.* **23** 213–9

Köhler B-U, Hennig C and Orglmeister R 2002 The principles of software QRS detection *IEEE Eng. Med. Biol. Mag.* **21** 42–57

Laguna P, Jané R and Caminal P 1994 Automatic detection of wave boundaries in multilead ECG signals: validation with the CSE database *Comput. Biomed. Res.* **27** 45–60

Laguna P, Mark R G, Moody G B and Goldberger A L 1997 A database for evaluation of algorithms for measurement of QT and other waveform intervals in the ECG *Comput. Cardiol.* **24** 673–6

Li C, Zheng C and Tai C 1995 Detection of ECG characteristic points using wavelet transforms *IEEE Trans. Biomed. Eng.* **42** 21–8

Martínez J P, Almeida R, Olmos S, Rocha A P and Laguna P 2004 A wavelet-based ECG delineator: evaluation on standard databases *IEEE Trans. Biomed. Eng.* **51** 570–81

McSharry P E, Clifford G D, Tarassenko L and Smith L A 2003 A dynamical model for generating synthetic electrocardiogram signals *IEEE Trans. Biomed. Eng.* **50** 289–94

Minhas F-u-A A and Arif M 2008 Robust electrocardiogram (ECG) beat classification using discrete wavelet transform *Physiol. Meas.* **29** 555–70

Moody G B 2008 The PhysioNet/computers in cardiology challenge 2008: T-Wave alternans *Comput. Cardiol.* **35** 505–8

Moody G B and Mark R G 1990 The MIT-BIH arrhythmia database on CD-ROM and software for use with it *Comput. Cardiol.* **17** 185–8

Moody G and Mark R 1982 Development and evaluation of a 2-lead ECG analysis program *Comput. Cardiol.* **9** 39–44

Pan J and Tompkins W J 1985 A real-time QRS detection algorithm *IEEE Trans. Biomed. Eng.* **32** 230–6

Patil S and Abel E W 2009 Real time continuous wavelet transform implementation on a DSP processor *J. Med. Eng. Technol.* **33** 223–31

Petrutiu S, Ng J, Nijm G M, Al Angari H, Swiryn S and Sahakian A V 2006 Atrial fibrillation and waveform characterization. A time domain perspective in the surface ECG *IEEE Eng. Med. Biol. Mag.* **25** 24–30

Proakis J G and Manolakis D G 1996 *Digital Signal Processing. Principles, algorithms and applications* 3rd edn (Englewood Cliffs, NJ: Prentice-Hall)

Sahambi J S, Tandon S N and Bhatt R K 1997 Using wavelet transforms for ECG characterization. An on-line digital signal processing system *IEEE Eng. Med. Biol. Mag.* **16** 77–83

Soria-Olivas E, Martínez-Sober M, Calpe-Maravilla J, Guerrero-Martínez J F, Chorro-Gascó J and Espí-López J 1998 Application of adaptive signal processing for determining the limits of P and T waves in an ECG *IEEE Trans. Biomed. Eng.* **45** 1077–80

Sörnmo L and Laguna P 2005 *Bioelectrical Signal Processing in Cardiac and Neurological Applications* (New York: Elsevier/Academic)

Speranza G, Nollo G, Ravelli F and Antolini R 1993 Beat-to-beat measurement and analysis of the R–T interval in 24 h ECG Holter recordings *Med. Biol. Eng. Comput.* **31** 487–94

Strumillo P 2002 Nested median filtering for detecting T-wave offset in ECGs *Electron. Lett.* **38** 682–3

Taddei A, Distante G, Emdin M, Pisani P, Moody G B, Zeelenberg C and Marchesi C 1992 The European ST-T database: standard for evaluating systems for the analysis of ST-T changes in ambulatory electrocardiography *Eur. Heart. J.* **13** 1164–72

Vila J A, Gang Y, Rodriguez Presedo J M, Fernández-Delgado M, Barro S and Malik M 2000 A new approach for TU complex characterization *IEEE Trans. Biomed. Eng.* **47** 764–72

Vullings H J L M, G. Vergaehen M H and Verbruggen H B 1998 Automated ECG segmentation with dynamic time warping *Conf. IEEE Eng. Med. Biol. Soc.* **1** 163–6

Yu S-N and Chen Y-H 2009 Noise-tolerant electrocardiogram beat classification based on higher order statistics of subband components *Artif. Intell. Med.* **46** 165–78